Contents lists available at ScienceDirect

Engineering Structures

Full scale testing of timber-concrete composite floors in an overhanging configuration

Javier Estévez-Cimadevila [*], Félix Suárez-Riestra, Emilio Martín-Gutiérrez, Dolores Otero-Chans

Univesity of A Coruña, Spain

A B S T R A C T

The behavior of timber-concrete composite floors in an overhanging configuration has been analysed. The floor consisted of a prefabricated T-shape piece formed by a glulam flange glued to a plywood rib and connected to an upper concrete slab poured in situ. The connection between both materials is achieved by penetrating the concrete into the holes made in the rib.

Three-point bending tests were performed with a total of 8 specimens with depth of 25, 30 and 35 cm and overhanging length of 1.50, 1.80 and 2.10 m, respectively. That means a length-to-depth ratio equal to 6 in all cases.

The experimental results showed that the lowest ultimate load value obtained was 8.03 and 5.55 times higher than the estimated service load for a building with residential use (5 kN/m^2) and public use (9 kN/m^2), respectively.

Two types of failure were observed after a marked cracking process in the concrete as the ultimate load value was approached: tensile failure affecting the plywood rib and shear failure at the glulam flange-plywood rib connection.

The maximum deflection for the total load was between 1/358 and 1/523 of the overhanging span for the estimated loads for a residential use building (5 kN/m^2), and between 1/266 and 1/390 for public use buildings (9 kN/m^2).

Regarding to vibrations, floors in an overhanging configuration with a length-to-depth ratio equal to 6 and a simply supported portion equal to four times the length of the overhanging portion, with total loads up to 9.0 kN/m^2, both in multi-storey buildings for residential and office use, present a high comfort level.

Consequently, the proposed timber-concrete composite (TCC) overhanging floor solution has demonstrated high stiffness and strength that make it a suitable alternative for the construction of high-performance light-weight floors in multi-storey buildings.

1. Introduction

The impact that construction has on CO_2 emissions [1] and the forecast of new increases [2] linked to the post-pandemic economic recovery and demographic growth, among other factors, is leading to the search for more ecologically efficient solutions. This entails a reduction in the use of the most used materials in the construction of structures (steel and concrete) and the growing importance of wood and its derived products, thanks to the effective combination of good mechanical properties with its well-known advantages from the point of view of sustainability [3–7].

On the other hand, the gradual introduction of wood in the construction of multi-storey buildings is increasing the use of this material and leads to the reflection that a massive use of it can lead to forest degradation due to the tendency towards monoculture of the most suitable species for use in the building sector [6,8].

One of the main problems that arise in the use of wood in the construction of framed structures for multi-story buildings is the difficulty of achieving rigid or semi-rigid joints. This reduces the stiffness of the assembly against horizontal wind or earthquake actions and, on the other hand, leads to the usual use of simply supported pieces, an inefficient solution both in terms of stiffness and strength that leads to an increase in material consumption. An interesting alternative to timber-only construction is the use of timber-concrete composite (TCC) solutions.
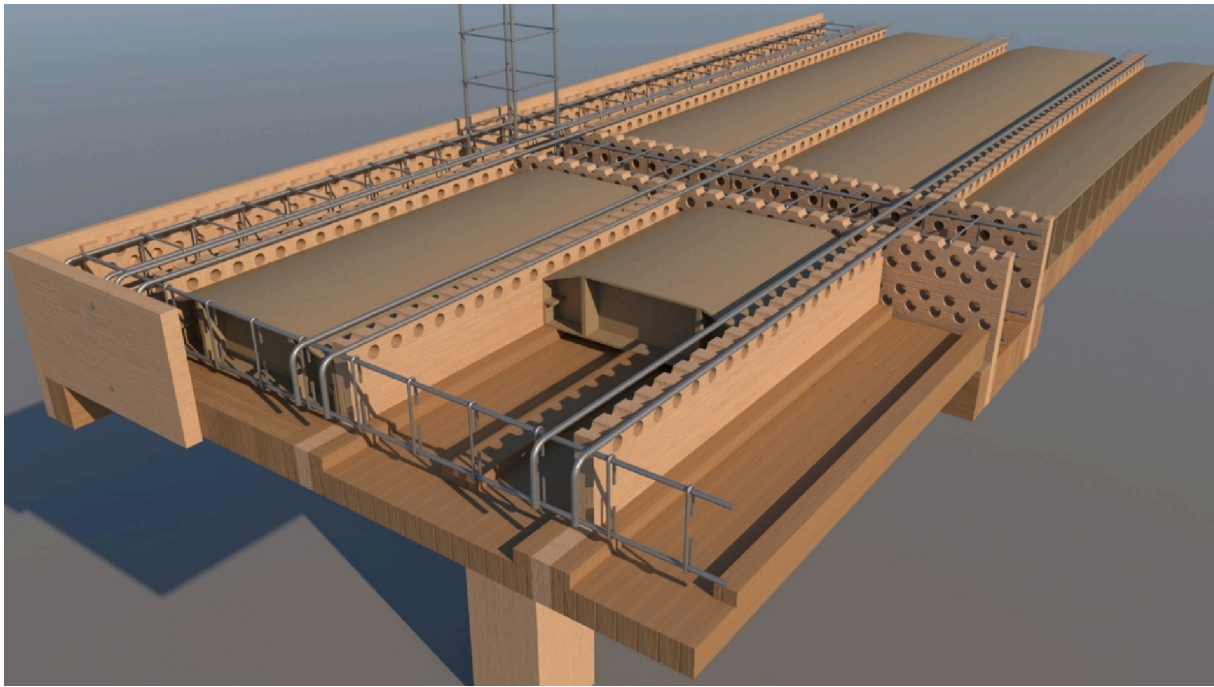
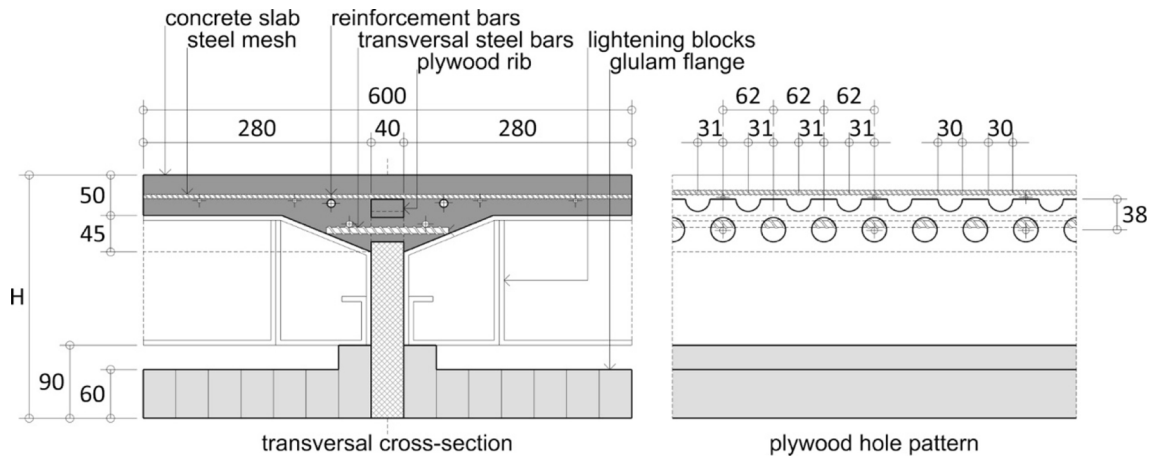**Fig. 1.** Three-dimensional model of the flooring system

Fig. 2. Specimen geometry. Dimensions in mm.

TCC systems provide greater structural efficiency than timber-only structures thanks to the synergy between both materials and, at the same time, allow a substantial improvement in terms of ecological efficiency compared to concrete-only structures. Many references address the advantages of TCC solutions [9–11].

Our team has patented a comprehensive construction system based on the use of TCC sections in floors, beams, and pillars [12] (Fig. 1). Floors and beams are made up of an inverted T-shape or inverted π-shape prefabricated piece formed with a glulam flange and rib boards made of perforated plywood. This prefabricated piece connects to a poured-in-place concrete top slab through existing holes in the plywood board. The behavior of TCC systems largely depends on the effectiveness of the timber-concrete shear connection, so that in addition to a high strength against shear forces, this is achieved with a reduced slippage of the joint, as this allows a high composite effect. The tests carried out by our team [13] have shown a high efficiency of the solution developed with perforated boards as a means of joining. Likewise, a four-point bending test has been carried out with pieces of 6.0, 7.20 and 8.40 m

spans that have shown excellent behavior both from a resistant point of view and against deformations and vibrations in service situations [14].

Previous papers about the developed system published by our team collect the analysis carried out linked to the positive bending moments behaviour. However, one of the great contributions of the patented TCC construction system is that it allows made up of semi-rigid beam-column joints and continuous floors over internal supports, working as continuous. It is a notable advance as it allows, in a multi-story structure, a much more favorable redistribution of bending moments and a notable reduction in deformations of the beams and floors. Consequently, it is essential to know the negative bending moments behavior of TCC systems in the field of new construction, analyzing the effect that it has on both the resistance of the shear timber-concrete connection using perforated boards, as well as on the stiffness and strength of the piece, when the concrete is subjected to tension stresses instead of the compression ones present in the usual TCC systems. It is a completely unexplored path as attested the very few references in the technical literature that address this issue [15,16], that, in any case, collects
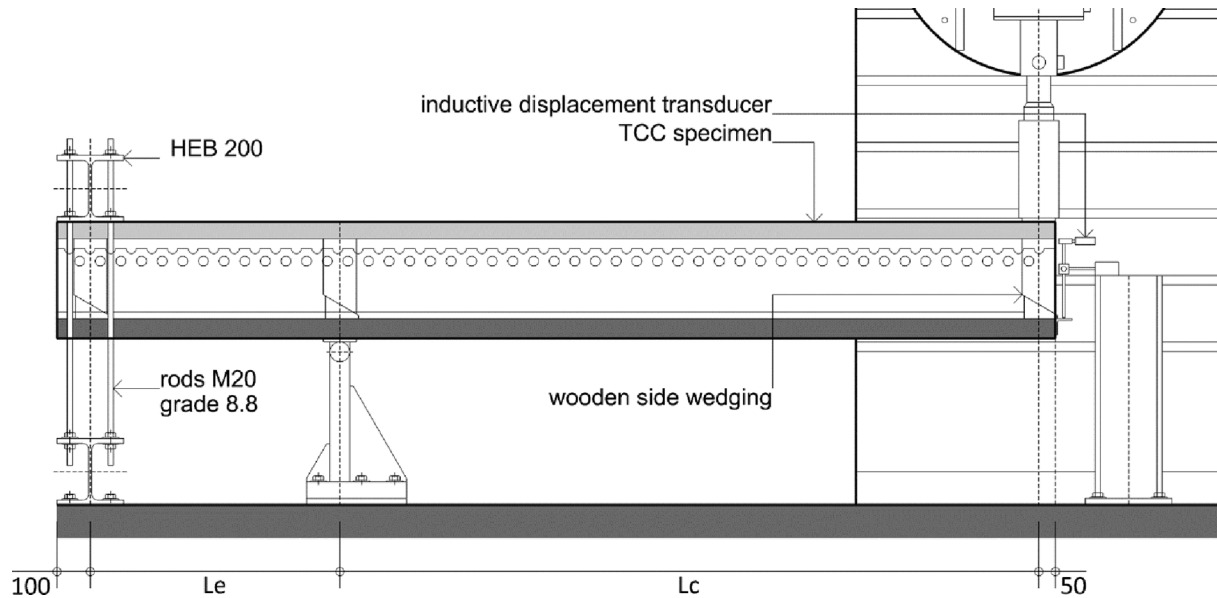
Fig. 3. Specimens manufacture

Fig. 4. Bending test

solutions more linked to the field of reinforcement of existing structures or far removed from the approaches included in this paper. Consequently, it has been considered essential to undertake a new experimental campaign, using full-scale pieces, that analyses the behavior of this type of pieces against negative bending moments, constituting the objective of this paper.

2. Materials and methods

2.1. Specimens and materials

The overhanging beam configuration tested (Fig. 2) is composed of a prefabricated T-inverted shaped piece formed of a glued laminated timber (GLT) flange glued to a rib made of plywood. The GLT flange is 600 mm wide and 60 mm thick which increases to 90 mm in the rib contact area to reduce glue line stresses. The rib has a thickness of 40 mm and was transversally perforated in its upper part with circular hollows of 30 mm in diameter to connect with a concrete layer poured over the light cardboard blocks. The concrete slab has a thickness of 50 mm, increasing to 95 mm in the connection area with the rib. A 200x200 mm steel mesh with 6 mm diameter corrugated bars has been placed on the concrete slab. Likewise, reinforcement bars 120 mm long and 10 mm diameter have been placed that go through one of every three rib perforations to provide ductility to the wood-concrete connection. Finally, since these are pieces intended for negative bending moment tests, 2 reinforcement bars of 10 mm have been placed, one on each side of the rib. The aforementioned reinforcement bars together with the 3φ6 of the

steel mesh parallel to the guideline of the piece gives rise to a total geometric amount of reinforcement for negative bending of 7.10^{-3} mm^2/mm^2. Fig. 3 shows different stages of the manufacturing process of the specimens.

The main mechanical properties of materials are the following.

The GLT flange was made of *Picea Abies* strength class GL24h, with mechanical properties according to standard EN 14080:2013 [17].

Birch plywood was chosen for the rib because high shear strength is required. According to manufacturer specifications, mean mechanical parameters parallel to the fibre of birch plywood are a characteristic compression strength of 26.5 N/mm^2; characteristic tension strength of 38.3 N/mm^2; mean MOE in bending of 8925 N/mm^2; mean MOR in shear of 650 N/mm^2, and a characteristic panel shear of 9.5 N/mm^2.

Reinforcement steel bars B500S quality were used with a yield strength $f_y \geq 500$ N/mm^2 and an ultimate tensile strength $f_u \geq 550$ N/mm^2 according to UNE 36068:2011 [18].

The upper slab was made using fibre-reinforced concrete, with 360 kg/m^3 of CEM II/A-M (V-L) 42.5 R cement [19] and a proportion of 4% Sikafiber Force M-48 (Sika®) polyolefin macrofibres of 48 mm long and 465 N/mm^2 tensile strength, according to EN 14889-2:2006 [20]. A fluid consistency has been used for the concrete, obtaining a 10 cm seat in the slump test according to [21]. An average strength at 28 days of 39.9 N/mm^2 was obtained in compression tests carried out according to EN 12390-3:2009 [22].

Based on the results obtained from the timber-concrete shear connection in a previous test campaign [13], a slip modulus K_{ser}=280 N/mm^2 and an ultimate load of F_u=285 kN/m have been considered.

Table 1
Load and displacement results of test campaign.

Specimen	L_c	Test phase 1				Test phase 2				Failure
		F_{SLS}	$F_{SLS,ave}$	w_{SLS}	$w_{SLS,ave}$	F_{ULS}	$F_{ULS,ave}$	w_{ULS}	$w_{ULS,ave}$	Modes
	[m]	[kN]	[kN]	[mm]	[mm]	[kN]	[kN]	[mm]	[mm]	Modes
250.1-X	1.50	6.55	6.54	9.15	8.73	54.62	52.09	124.62	117.62	FM1
250.1-Y		6.57		8.76		47.01		116.62		FM2
250.2-X		6.51		8.27		54.64		111.63		FM2
300.1-X	1.80	7.30	7.37	11.19	10.61	42.69	51.10	86.92	113.41	FM2
300.2-X		7.47		10.05		56.43		128.37		FM1
300.2-Y		7.35		10.58		54.19		124.93		FM1
350.2-X	2.10	8.16	8.14	12.76	12.77	51.82	48.59	119.58	108.27	FM2
350.2-Y		8.12		12.78		45.36		96.96		FM2

FM1. Pronounced cracking of the concrete and failure due to tension in the rib.

FM2. Pronounced cracking of the concrete and shear failure in the GLT flange and rib connection.
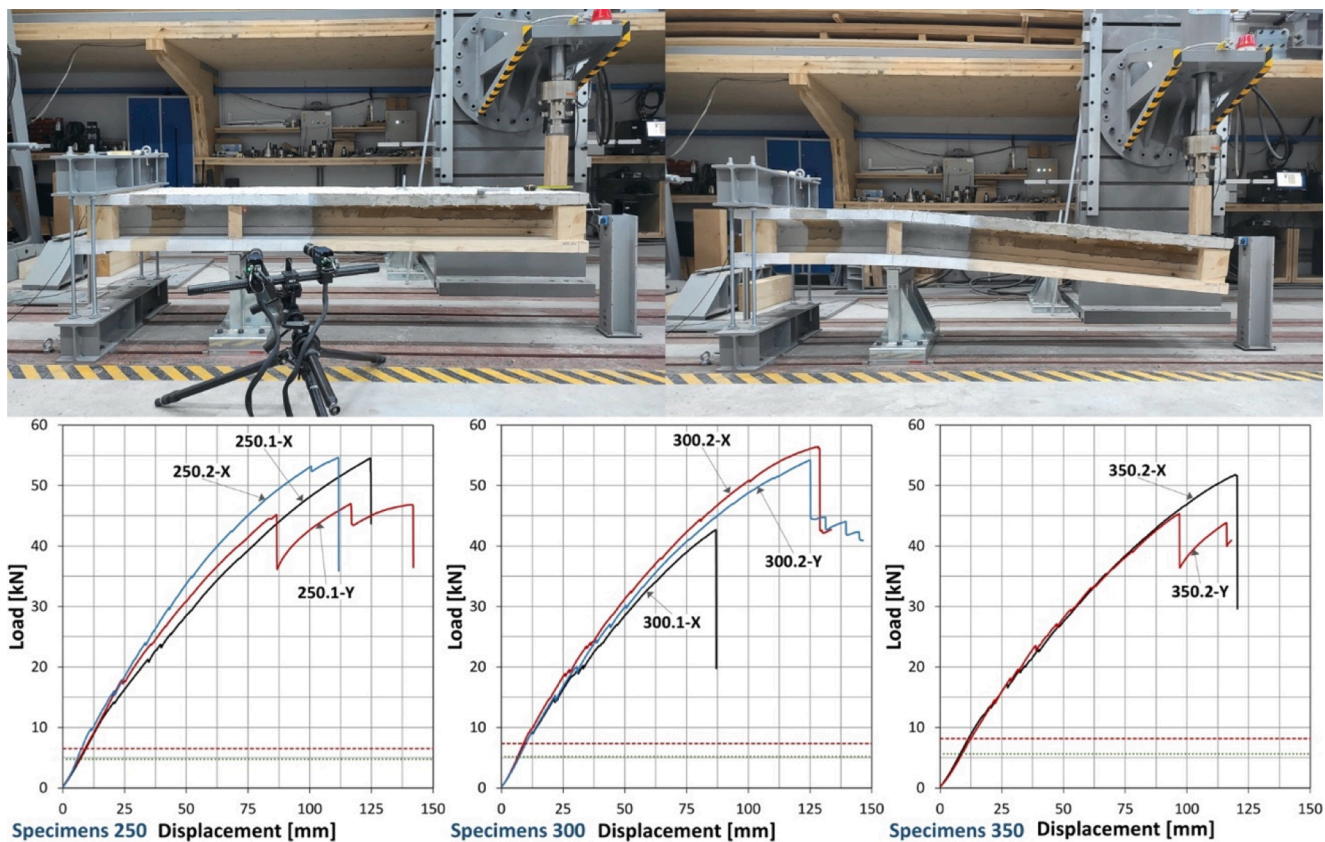
Fig. 5. Bending test and load-displacement curves test phase 2. Point load equivalent to a service load of 5.0 kN/m² and an enclosure load of 2.5 kN (dot line). Point load equivalent to a service load of 9.0 kN/m² and an enclosure load of 2.5 kN (dashed line).

2.2. Test-setup

A total of 8 samples obtained using the undamaged extreme quarters of the beams tested in previous four-point bending tests [14] were tested. For the names of the samples, in order to identify their origin, they are referenced in the same way as the piece from which they were extracted, adding the letters "X" and "Y" to identify both ends. In total, 8 pieces were tested: 3 with a depth of 250 mm and a overhanging span (L_c) of 1.50 m; 3 with a depth of 300 mm and a span of 1.80 m and 2 pieces with a depth of 350 mm and a span of 2.10 m. A slenderness of L_c/6 has been adopted for all the pieces based on the stiffness results obtained with a simplified preliminary design analytical model. This model was based on the use of the Gamma Method, a simplified method outlined in Eurocode 5–Annex B [23] and usually recommended [24,25] for TCC sections. In this case, as they are cantilevered pieces, an effective

length equal to $2L_c$ has been considered. Likewise, the contribution of the negative reinforcement has been considered and the tensile contribution of concrete has been dispensed with.

Before the start of the tests, wedging was carried out between the concrete slab and the glulam flange in the support and load application areas. The mentioned wedging was intended to prevent possible load eccentricities from affecting the result, moving away from the real behavior of the system, since in the specimens the concrete slab is cantilevered in a transverse direction while in reality it works in continuity between the different ribs that make up the floor.

Three-point bending tests were performed with a PB2-F/600 Microtest hydraulic machine (Fig. 4). Vertical displacement was measured at the end of the overhanging beam using a Schreiber SM160.100.2.ST inductive displacement transducer. In addition, an Aramis 3D sensor was used to apply Digital Image Correlation (DIC) to

Fig. 6. Failure modes.Samples: 250.1-X (a, b, d); 250.2-X(h); 250.1-Y(g); 300.1-X(i); 300.2-X(e); 300.2-Y(b, f); 350.2-X(j). Note: images e, g, i show the remains of cardboard corresponding to the vaults used as lightening elements and that were partially removed to observe the damage to the wood

analyze displacements and strains without contact.

A test with two phases were performed on each specimen.

• Test phase 1. Test until the service load is reached (F_{SLS}). To estimate this load value, a permanent uniformly distributed load of 2.0 kN/m^2 of the structure's self-weight, 2.0 kN/m^2 of finishes, and a variable load of 5.0 kN/m^2 corresponding to public use (category C5 Euro-code 1 [26]) has been considered. To determine the load to be applied to the load cell, it was decided to consider the total load (9.0 kN/m^2), without discounting the self-weight of the piece, in order to measure the deformations of the element under the total design load. In addition to the indicated permanent uniformly distributed load, the action of a possible enclosure arranged at the free end of the cantilever with a value of 2.50 kN has been considered. Consequently, the load to be applied at the end of the cantilever, equivalent in terms of maximum bending moment to the joint action of the surface load and the load of the enclosure, is 6.55 kN, 7.36 kN and

Table 2
Experimental deflections for different service loads.

	Q_{total}= 3.0 kN/m² $P_{closing}$=2.5 kN		Residential use building Q_{total}= 5.0 kN/m² $P_{closing}$=2.5 kN				Public use building Q_{total}= 9.0 kN/m² $P_{closing}$=2.5 kN				Stiffness	
	F_3	w_3	F_5	w_5	$w_{5,ef}$	$w_{5,ef}$	F_9	w_9	$w_{9,ef}$	$w_{9,ef}$	EI_t	$EI_{t,ave}$
	[kN]	[mm]	[kN]	[mm]	[mm]	relative	[kN]	[mm]	[mm]	relative	[kN·m²]	[kN·m²]
250.1-X	3.62	4.64	4.36	5.58	4.00	L_c/375	5.85	7.44	5.37	L_c/279	1717	1928
250.1-Y		4.45		5.51	4.20	L_c/358		7.40	5.63	L_c/266	1607	
250.2-X		3.80		4.43	2.87	L_c/523		5.73	3.85	L_c/390	2847	
300.1-X	3.82	4.75	4.70	5.75	4.07	L_c/443	6.46	7.73	5.59	L_c/322	3194	3218
300.2-X		4.12		5.14	3.83	L_c/470		6.91	5.26	L_c/342	3485	
300.2-Y		4.42		5.65	4.24	L_c/424		7.54	5.83	L_c/309	3009	
350.2-X	4.02	4.83	5.03	6.16	4.96	L_c/424	7.05	8.64	6.95	L_c/302	4211	4089
350.2-Y		5.34		6.65	5.18	L_c/406		9.33	7.26	L_c/289	3974	

8.17 kN for overhanging spans of 1.50 m, 180 m and 2.10 m, respectively.

- Test phase 2. Test until reaching the failure load (F_{ULS}).

3. Results and discussion

3.1. Ultimate load and failure modes

Table 1 shows the load and displacement results of the 8 tested specimens. Fig. 5 shows the test image of one of the specimens, as well as the load-displacement curves of the tested pieces.

One of the first questions that can be raised is the effect that possible damage to materials and connections of the pieces may have on the results obtained due to the previous bending tests carried out. It is evident that the reuse of previously tested parts has been due to an attempt to optimize the available resources given the high cost of manufacturing large pieces. In previous tests, the displacements were recorded using Digital Image Correlation, observing that the slippage was only significant at both ends of the specimen 250.1. In any case, the ultimate load values reached in the mentioned bending tests correspond to a shear at the ends of the piece far from the values obtained in the shear tests carried out in a previous experimental campaign [13]. Consequently, it was understood that the possible hidden damages would not be meaningful enough to significantly affect the results obtained and, in any case, would still make the results obtained more favourable.

As stated above, the specimens 250.1 exhibited significant slab slippage at both ends. Despite the magnitude of the slip (Fig. 6-a), no meaningful variations were observed in specimens 250.1-X and Y in terms of ultimate load and only a clear reduction in stiffness should be appreciated for values higher than the service load (Fig. 5 and Table 2).

In order to properly assess the ultimate load values obtained experimentally, it is convenient to compare these values with those expected in a real situation with service loads. Two representative situations have been considered. On the one hand, a building for residential use and light finishes with a total load of 5.0 kN/m² (2.0 kN/m² of the structure's self-weight, 1.0 kN/m² of finishes and a variable imposed load of 2.0 kN/ m²). Additionally, a point load corresponding to the enclosure of 2.5 kN has been considered. The other service situation considered is that of a building for public use with a total load due to use of 9.0 kN/m² (2.0 kN/m² self-weight of structure, 2.0 kN/m² of finishes and imposed load variable use load of 5.0 kN/m²), to which is added the same enclosure load at the free end. This second service situation corresponds to the loads applied in test phase 1. Establishing the equivalence, in terms of maximum bending moment, between the uniformly distributed loads considered (real situation of the structure) and the point load applied at the end of the cantilever (test situation), the following correspondence is obtained: 4.75 kN and 6.55 kN for L_c=1.50 m span, 5.20 kN and 7.36 kN for L_c=1.80 m and 5.65 and 8.17 kN for L_c=2.10 m (these values have been represented in the load-deflection curves of

Fig. 5). If we compare these values with the F_{ULS} values of ultimate load obtained (Table 1), we observe that, considering the lowest value of each series, the ultimate load for L_c=1.50 m is 9.90 and 7.18 times the estimated service load for residential and public use buildings, respectively. In the case of L_c=1.80 m, these coefficients become 8.21 and 5.80. Finally, for L_c=2.10 m, values of 8.03 and 5.55 are obtained. It can be seen, therefore, that the lowest value obtained is 5.55 times higher than the design value of a building with loads for public use, which demonstrates the high bearing capacity of the solution.

Attending to the failure mode, in all cases it has been observed that when approaching the ultimate value, a marked cracking process begins in the concrete with cracks of increasing opening as the load increases and the support is approached, with a transverse path to the longitudinal axis of the piece (Fig. 6-b, c). The failure is reached abruptly and suddenly, observing two types of failure. In three of the specimens, the failure was caused by tension that affected the plywood rib (Fig. 6-d, e, f). In the remaining five, shear failure occurred at the connection of the glulam flange with the plywood rib (Fig. 6-g, h, i, j).

If the failure modes are analysed in relation to the ultimate loads with which they are reached, it can be seen that the load values that lead to both types of failure are very similar, which indicates an adequate dimensioning of the elements that make up the section as there is no a single resistant mechanism that precipitates the failure. Obviously, this assessment cannot be completely conclusive due to the number of specimens tested and because they are reused pieces from previous tests until failure, which may, therefore, have some type of internal damage not observed.

In relation to the cracking of the concrete that has been observed in the tests, it should be noted that the objective of crack control, included in all the regulations, is to guarantee that the opening of the cracks is below a certain threshold that is established based on the environmental conditions in which the structure is located. In the Eurocode 2 [27] the maximum crack opening is 0.4 mm for inside buildings with low air humidity, a value that is reduced to 0.3 mm for inside buildings with moderate or high air humidity or external concrete sheltered from rain. Therefore, the first question is not so much that cracking does not occur, but that the cracking is within those regulatory limits. The aforementioned limitations correspond to the opening of the cracks obtained for the quasi-permanent load combination, and the way to effectively controlled it, is to reduce the elongation of the reinforcements and, therefore, their tension stress, which is easily achieved by increasing the amount of reinforcement.

Fig. 5 of the paper shows the point loads equivalent to a total service load of 9 kN/m² (2.0 kN/m² self-weight, 2.0 kN/m² of finishes and 5.0 k/m² of variable load for public use) and a load of 2.50 kN applied at the free end corresponding to a possible enclosure. Point load values obtained are 6.55 kN, 7.36 kN and 8.17 kN for the overhaning spans of 1.50 m, 1.80 m and 210 m, respectively. These values are reduced, for the referred spans, to 4.12 kN, 4.44 kN and 4.77 kN for the quasi-permanent combination for light finishes (1 kN/m²) and residential use, and 5.65

Table 3
Mean values of rotation angle at the support (Φ), bending deflection (w_b) and shear deflection (w_{sh}) for different service loads.

	Residential use building Q_{total}= 5.0 kN/m² $P_{closing}$=2.5 kN				Public use building Q_{total}= 9.0 kN/m² $P_{closing}$=2.5 kN			
	Φ	w_b	w_{sh}	$w_b/ (w_b +w_{sh})$	Φ	w_b	w_{sh}	$w_b/ (w_b +w_{sh})$
	[rad].10^{-3}	[mm]	[mm]	%	[rad].10^{-3}	[mm]	[mm]	%
250	0.92	2.54	1.14	31.0	1.24	3.41	1.53	31.0
300	0.57	2.84	1.21	29.8	0.79	3.90	1.66	29.8
350	0.45	3.80	1.27	25.1	0.63	5.32	1.78	25.1

kN, 6.28 kN and 6.91 kN for the quasi-permanent combination in the case of public use. It can be seen in the paper displacement curve graphs (Fig. 5) that these load values find in a completely linear phase of behavior. Under these conditions, as long as the cracking of the concrete does not start, the analytical model using the gamma method allows us to know the distribution of stresses in any cross section of the piece. The maximum tension stress obtained considering load values corresponding to public use buildings, which is the most unfavorable situation, are 2.67 N/mm², 2.35 N/mm² and 2.22 N/mm² for the overhaning spans of 1.50 m, 1.80 m and 210 m, respectively. These values are clearly below the tension resistance of concrete with fibers obtained in tests, which was 4.00 N/mm², which means that no type of cracking occurs. Even assuming that the concrete did not have the addition of fibers, the tension resistance according to Eurocode 2 would be 2.9 N/mm², higher than the tension stresses obtained corresponding to the most unfavorable hypothesis.

These results correspond to what was observed during the tests where no type of cracking was observed up to values higher than those of the service load. And, in any case, as already indicated, the possible cracking would not be a problem as long as its opening did not reach the limits set by the regulations, an issue easily controllable with the amount of the reinforcement provided.

Another question to be raised with the test results is that the failure behavior was quite brittle. This type of failure is characteristic of bending failure due to tensile breakage of the timber fibers. As the bending moment of failure approaches, pops begin to be heard corresponding to the first fibers that begin to break before the failure of the beam. In the tests carried out, the brittle failure occurred in all pieces, since either it started in some pieces with the breaking of the fibers in the board, or due to a shear failure in the connection of the birch plywood with the GLT flange in others, mechanisms that in both cases lack ductility, so that failure, when it is reached, occurs abruptly.

In any case, it should be noted that the lowest value obtained of ultimate load was 5.55 times higher than the design value of a building with loads for public use, and 8.03 times in the case of residential use. Therefore, the level of security far exceeds regulatory requirements.

On the other hand, we have indeed thought of a solution that will undoubtedly improve the ductility of the system's behavior. In the tests carried out, the board is continuous throughout the length of the piece. This means that in the section corresponding to the interior support the board is highly tensioned, which gives rise to sudden and brittle failure. However, in the proposed solution of cantilever floors and continuous floors over several supports, the floors located on each side of the beam support independently on it, so the board is interrupted, as can be seen in Fig. 1. In this way, the negative bending moment in the support section is resisted only by tension in the reinforcement bars and compression in the GLT flange, leaving the board as an element whose main function is to transmit the shear forces. Given that the shear failure of the connection board-concrete is ductile, as the tests we have carried out have shown [13], we understand that the progressive cracking of the concrete will allow a ductile failure and a redistributive capacity of the bending moments.

3.2. Bending stiffness

Tables 2 and 3 collect the displacement values corresponding to the two situations analysed: a building for residential use (total uniform distributed load of 5.00 kN/m² and enclosure load at the point of 2.50 kN) and a building for public use (total uniform distributed load of 9.00 kN /m² and enclosure load at the end of 2.50 kN). In addition, another load situation (3 kN/m² and enclosure of 2.50 kN) has been added in order to determine the stiffness of the element in a representative section of the load-displacement curve. The values w_3, w_5, w_9 indicate the displacement value at the free end for each of the load situations analysed. To determine the bending stiffness of the overhanging beam, it must be considered that the double support system does not achieve a completely effective simulation of the embedment. To take this effect into account and determine the real deflection of the piece due to the bending induced by the load, the effective value of the displacement at the free end (w_{ef}) has been determined, discounting to the total displacement at the free end the displacement due to the rotation produced in support.

The Table 2 also includes the effective bending stiffness (EI_t) calculated using Eq. (1), in which the deformation due to shear stress has been taken into account, the magnitude of which is significant as it is a short piece with a point load applied in the free end. L_c is the cantilever span; L_e is the distance between supports; G is the transverse elastic modulus of the rib (650 N/mm²); A_s the effective area at shear stress with values of 40x220 mm², 40x270 mm² and 40x320 mm² for specimens of 250 mm, 300 and 350 mm height, respectively; F_9 is the point load equivalent, in terms of maximum deflection, to the load hypothesis considered corresponding to a building for public use (9 kN/m²) and an additional enclosure load of 2.5 kN, F_3 is the point load equivalent to an uniformly distributed load of 3.0 kN/m² and the same additional enclosure load and (w_9-w_3) is the increase of deformation for the given load variation.

$$EI_t = \frac{L_c^2(L_c + L_e)}{3\left[\frac{(w_9 - w_3)}{(F_9 - F_3)} - \frac{L_c}{GA_s}\right]} \tag{1}$$

As can be seen in the Table 2, the relative total deflection values are between $L_c/358$ and $L_c/523$ for a load of 5.0 kN/m² and between $L_c/266$ and $L_c/390$ for a load of 9.0 kN/m². In the Eurocode 5 [23] a limitation range is established for the instantaneous deflection of overhanging beams from $L_c/150$ to $L_c/300$, establishing the national annexes of the Eurocode for greater precision. The Spanish annex establishes the value of $L_c/150$. Consequently, it is observed that the results obtained are clearly satisfactory in terms of both the integrity of the construction elements and the comfort of the user.

Table 3 shows the average values of the bending and shear deflections for each type of specimen, as well as the percentage that shear deflection represents in the total deflection. The high repercussion that shear deformation has on the total deformation, clearly higher than that obtained in building structures with other materials, is a consequence of several factors. The first is that the tested pieces have a reduced span and a point load was applied to them at their free end. It is a configuration in which the repercussion of the shear deformations is clearly higher compared to pieces with a larger span and uniformly distributed loads.
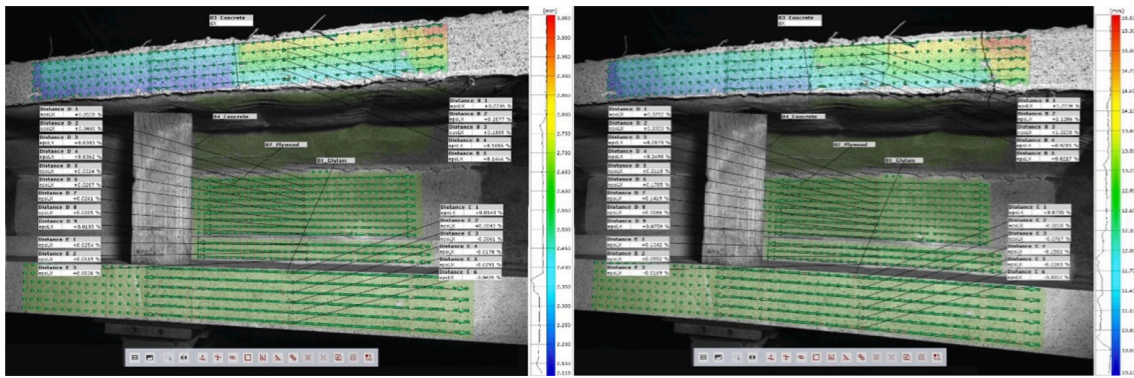
Fig. 7. DIC analysis of specimen 300.2-Y corresponding to a load of 15.32 kN and 54.19 kN
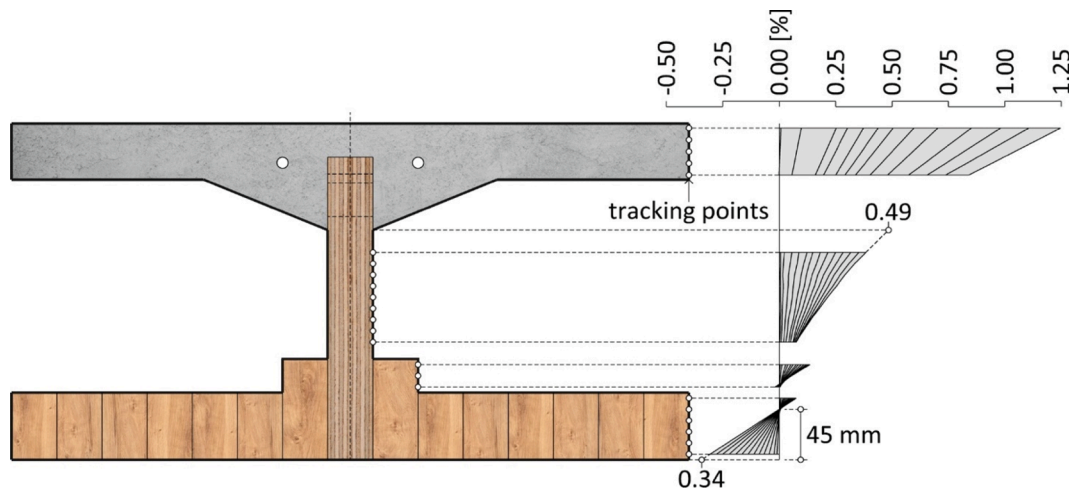

Fig. 8. Strain distributions of the support section of specimen 300.2-Y obtained by DIC for different load values
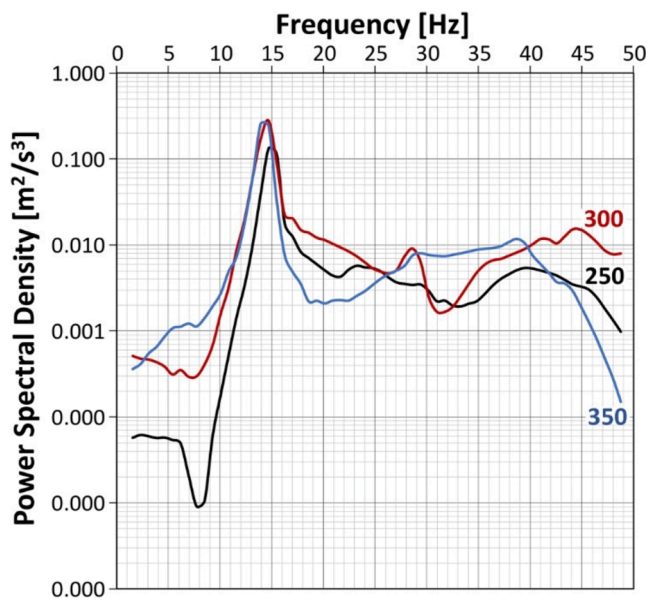

Fig. 9. Curves PSD-Frequency

Table 4
Floor vibration criteria according to floor performance level [31].

Criteria	Floor performance levels						
	I	II	III	IV	V	VI	VII
Stiffness criteria for all floors w_{1kN} [mm] $\leq$	0.25	0.25	0.5	0.8	1.2	1.6	no criteria
Response factor $R \leq$	4	8	12	16	24	32	
Frequency criteria for all floors f_1 [Hz] $\geq$	4.5						
Acceleration criteria for resonant vibration design situations a_{rms} [m/s^2] $\leq$	0.005 R						
Velocity criteria for transient vibration design situations v_{rms} [m/s] $\leq$	0.0001 R						

Table 5
Recommended selection of floor performance levels [31].

Use category		Quality choice	Base choice	Economy choice
A (residential)	Multi-storey	level I, II, III	level IV	level V
	Single house	level I, II, III, IV	level V	level VI
B (office)		level I, II	level III	level IV

Secondly, the birch plywood board has a low MOR value (650 N/mm2) compared to MOE (8925 N/mm2). Finally, a rib with a reduced thickness (40 mm) has been used, which increases the shear stresses and, consequently, its deformation.
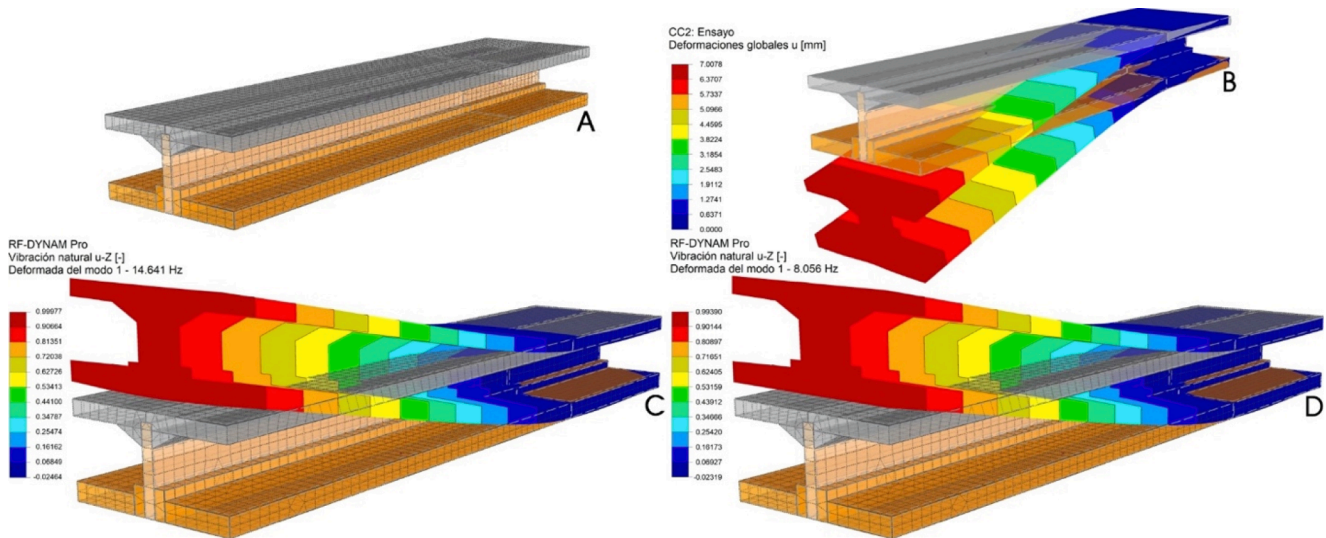
Fig. 10. FEM analysis of specimen type 300. Thickness 300 mm. L_c=1.80 m. A-Meshed. B-Deformation for 9.0 kN/m^2 and 2.50 kN at the free end of the overhanging beam. C-Frequency for selfweight. D-Frequency for 9.0 kN/m^2 and 2.50 kN the free end of the overhanging beam.

The deformational behavior of the support section, in which the maximum bending moment is located, has been analysed by means of DIC. Fig. 7 shows the tracking points and inspection labels corresponding to two stages of the loading process. The first of them corresponds to an applied load of 15.32 kN (equivalent to a uniformly distributed load of 23.74 kN/m^2 + enclosure of 2.50 kN) to which a displacement at the free end of 21.47 mm corresponds. The second stage corresponds to the moment just before the failure reached with a load of 54.19 kN (equivalent to 95.72 kN/m^2 + enclosure of 2.50 kN) and a displacement of 124.93 mm.

Fig. 8 shows the strain distribution in the analysed points of the section for different load values. It can be seen that the resulting position of the neutral axis is located 45 mm from the lower edge of the piece, which means that practically the entire GLT flange is under compression stresses with normal strain values far shorter than the failure values. In an opposite way, the plywood rib in the area where it meets the concrete has reached a normal strain of 0.49% with a tensile stress of 45.09 N/mm^2 obtained considering the global MOE of the board of 9296 N/mm^2. These values fully justify the experimental reality observed with a breakage of the piece initiated in the upper part of the rib. On the other hand, the elongation experienced in the fibre corresponding to the position of the negative reinforcement bars has been 1%, which indicates that the bars are completely in the elastic phase.

3.3. Vibrational behavior

In order to complete the analysis of the behavior in service of the cantilever floors, it has been considered essential to know the dynamic response of the pieces. To this end, an experimental analysis of the behavior against the limit state of vibrations has been carried out. The experimental analysis has been carried out on a specimen of each of the lenghts used. Specimens 250.2-X, 300.2-Y and 350.2-Y have been analysed. The procedure consisted of exciting the system by an impulse reached by hitting with an instrumented hammer and measuring the response with a Bosch Sensortec BMI160 inertial measurement unit. The results obtained considering only the self-weight of the pieces, were natural vibration frequencies of 15.0, 14.6 and 14.0 Hz for the spans of 1.5, 1.8 and 2.1 m, respectively (Fig. 9).

In order to know the behavior of the pieces in real load situations, they were analysed using the RF-/DYNAN Pro natural vibrations Add-on Module for RFEM (Dlubal Software GmbH 024396 License), based on modal decomposition (modal analysis). This add-on determines the lowest eigenvalues of the model with a direct import of masses from load cases. A previous analysis was carried out to achieve an adequate model that reproduces the test estimated properties. An analytical model was applied to estimate the stiffness in relation to the natural frequencies (f_1) obtained in test, considering the supporting conditions (Eq. (2)).

$$f_1 = \frac{1}{2\pi} \sqrt{\frac{3EI}{0.24\mu L_c^4}} \tag{2}$$

Where μ represent the equivalent mass from self-weight (kg/m^2)

This stiffness was transferred to a deflection analysis, achieving a second comparative value with respect to the deflection test results.

These calibrated models, equivalent to the 250.2-X, 300.2-Y and 350.2-Y samples, are considered in a vibration serviceability behavior taken into account the described two load configurations, residential consideration (total load of 5.0 kN/m^2) and public spaces (total load of 9.0 kN/m^2) and, in both cases, an additional end load due to the enclosure of 2.50 kN was considered.

The Eurocode Basis of structural design [28] describes the principles and requirements for safety, serviceability and durability of structures. In relation to dynamic actions and serviceability limit states, the Eurocode Basis of structural design establish that vibrations must be considered as they can cause discomfort or affect the functional effectiveness of the structure. The Annex A1, Application for Buildings, determines that for the serviceability limit state of a structure or a structural member not to be exceeded when subjected to vibrations, the natural frequency of vibrations of the structure or structural member should be kept above appropriate values which depend upon the function of the building and the source of the vibration. In relation to these limitations, the Eurocodes give only recommendations for estimated limits for eigenfrequencies, e.g. 3 Hz or 8 Hz depending on the construction material, or they give reference to ISO-standards as ISO 10137 [29] and ISO 2631 [30], which give general criteria for the perception of vibrations and could be the basis to develop more detailed design rules for vibrations specific to particular structures and types of excitation. Eurocode 5 [23] deals specifically with the design of timber buildings and contains a chapter on vibrations in timber floor structures which could be found in Appendix G. In this standard 8 Hz fundamental frequency is established as a limit value, so an special investigation should be made for values under this limit.

The revised EC5 [23], developed by SC5/WG3 subgroup 7 [31] on Floor Vibrations and Design Floor Structures for Human Induced Vibrations [32] (considered as a supplement to EN 1990 [28]) incorporates a new vision about vibration effects in relation to comfort

Table 6
Response factor R and floor performance levels for overhanging floors with adjacent span of L_e=0.75 m.

Case	Mass	Stiffness		Eigenfrecuency			Velocity Criteria								Acceleration Criteria			Comfort
	μ	M*	EI	Analytical	FEM		I_m	$V_{1,peak}$	K_{imp}	ξ	η	β	V_{rms}	R	α	a_{rms}	R	Level
	[kg/m²]	[kg]	[N·m²]	[Hz]			[N.s]	[m/s]		[%]			[mm/s]			[mm/s²]		
250.Q5	1060.7	1099	880964	7.21	8.10		4.94	0.0032	1.00	3.50	0.97	0.482	1.52	15.17				IV
250.Q9	1190.7	1274		6.80	7.70										0.046	102.02	20.40	V
300.Q5	937.3	1156	1670125	7.33	7.91										0.042	103.37	20.67	V
300.Q9	1067.3	1355		6.87	7.28										0.054	113.47	22.69	V
350.Q5	849.1	1214	2598694	7.06	7.27										0.055	127.19	25.43	VI
350.Q9	979.1	1436		6.57	6.83										0.065	128.19	25.64	VI

assessment. It applies to floors in office and/or residential buildings that might be excited by human activity and which can affect the comfort of other building users. Both documents are focused on the evaluation of the response against human induced vibration, categorizing the structural response in terms of adequate comfort levels. The first document establishes a vibration criteria organized in six floor performance levels. Table 4 sets a series of requirements in relation to the vibration behavior, so further investigations are necessary if these requirements are satisfied. In addition, Table 5 determines recommendations to select and adequate comfort level in relation to the destination or use of the floor and the expected quality of construction.

These considerations are of interest to this case, since analysis parameters are established that comprise composite system. In this way, a modal damping (ξ) ratio of 2.5% is proposed for timber-concrete floors (3.5% for timber-concrete with a floating layer). The method fixes that the floor mass may include that caused by the quasi-permanent value of the distributed imposed loads, and recommends to limit this additional mass to 10% of the total imposed load. The analysis determines a response factor R that allows to classify in a level associated to a comfort category.

For transient vibration design situations, floors with a natural eigenfrequency greater than 8.0 Hz, the velocity criteria determines the response factor R, that is obtained according to the Eq. (3):

$$R = \frac{V_{rms}}{0.0001} \tag{3}$$

The root mean square velocity (V_{rms}) must be calculated according to the Eq. (4):

$$V_{rms} = \beta \cdot K_{imp} \cdot K_{red} \cdot \frac{I_m}{M^*} \tag{4}$$

Where

$$K_{imp} = \max \begin{cases} 0.48 \cdot \left(\frac{b}{L}\right) \cdot \left(\frac{EI_y}{EI_x}\right)^{0.25} \\ 1.0 \end{cases} \tag{5}$$

$$\eta = \begin{cases} 1.52 - 0.55 \cdot K_{imp} & when \quad 1.0 \leqslant K_{imp} \leqslant 1.5 \\ 0.69 \ else \end{cases} \tag{6}$$

$$\beta = (0.65 - 0.01 \cdot f_1) \cdot (1.22 - 11.0 \cdot \zeta) \cdot \eta \tag{7}$$

$$I_m = \frac{42 \cdot f_w^{1.43}}{f_1^{1.3}} \tag{8}$$

$$M^* = 0.64 \cdot \mu \cdot L \tag{9}$$

K_{imp} is the impulsive multiplier factor; K_{red} is a reduction factor (0.7), taking into account that the exciting source on the floor and the sensing person are at a distance from each other; I_m is the mean modal impulse (N.s); f_w is the walking frequency (1.5 Hz); M^* is the floor modal mass (kg); and μ is the total mass of the floor area (kg/m²). A modal damping ratio (ξ) of value 0.035 was adopted.

There is a second condition in relation to natural frequencies under 8.0 Hz. In this case a resonant floor is considered and an acceleration criterion is used. The root mean acceleration (a_{rms}) is obtained according to the Eq. (10):

$$a_{rms} = \frac{0.4 \alpha F_0}{2\sqrt{2} \xi M^*} \tag{10}$$

Where:

$\alpha = e^{-0.4 \cdot f_1}$ is the Fourier coefficient

F_0 is a vertical load from the person giving rise to the disturbance, set to 700 N

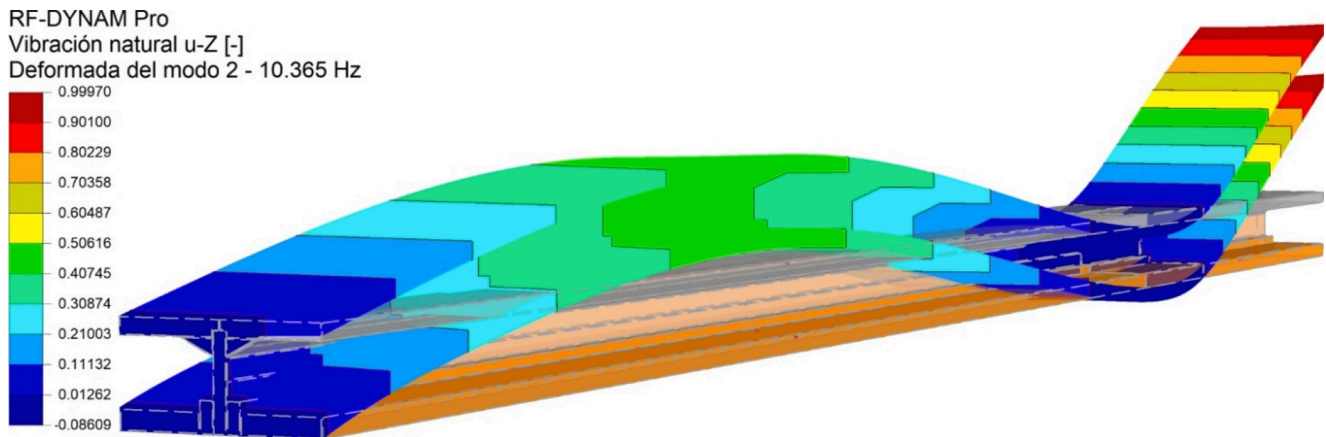The response factor (R) for the acceleration criteria is obtained

Fig. 11. FEM analysis of specimen type 300. Thickness 300 mm. L_c=1.80 m. L_e=4L_c. Frequency for 9.0 kN/m^2 and 2.50 kN at the free end of the overhanging beam.

Table 7
Response factor R and floor performance levels for overhanging floors with adjacent span of L_e=4L_c.

Case	Span		Mass	Eigenfrecuency		Velocity Criteria									Comfort
	L_e	L_c	M^*	FEM		I_m	$V_{1,peak}$	K_{imp}	ξ	η	β	V_{rms}	R		Level
	[m]	[m]	[kg]	[Hz]		[N.s]	[m/s]		[%]			[mm/s]			
250.Q5	6.0	1.5	2106	11.89		3.00	0.0010	1.00	3.50	0.97	0.430	0.429	4.29		II
250.Q9	6.0	1.5	2691	10.53		3.52	0.0009	1.00	3.50	0.97	0.441	0.403	4.03		II
300.Q5	7.2	1.8	2394	10.37		3.59	0.0010	1.00	3.50	0.97	0.443	0.464	4.64		II
300.Q9	7.2	1.8	3096	9.04		4.29	0.0010	1.00	3.50	0.97	0.453	0.439	4.39		II
350.Q5	8.4	2.1	2683	9.27		4.15	0.0011	1.00	3.50	0.97	0.451	0.489	4.89		II
350.Q9	8.4	2.1	3552	8.02		5.01	0.0010	1.00	3.50	0.97	0.462	0.462	4.62		II

according to the Eq. (11):

$$R = \frac{a_{rms}}{0.005} \qquad (11)$$

The analytical evaluation is complemented with the numerical FEM models previously calibrated, obtaining the eigenfrequency for each combination, simple depth, and load consideration. Fig. 10 collects the model corresponding to the pieces with a depth of 300 mm and span L_c=1.80 m. From each reference value of natural frequency, the response factor (R) is determined, and the corresponding level is established, allowing to determine the comfort response of the floor (Table 6).

The results obtained from the response factor (R) indicate a low floor performance level that corresponds to the so-called economy choice. This is a consequence of the use of a FEM model that simulates the behavior of the experimental specimens (Fig. 4) but not that of the usual structural typologies. In a real structure, the length of the span adjacent to the cantilever is usually greater than the 0.75 m separation between supports of the tested pieces. For this reason, new FEM analyses have been carried out using spans with a separation between supports equal to 4 times the span L_c of the overhanging floor (Fig. 11); that is, spans with a slenderness L_e/24 in correspondence with overhanging floors with a slenderness L_c/6. The results are collected in Table 7 in which the eigenfrequencies corresponding to vibration mode 2 associated with the most unfavourable situation of the cantilever are indicated.

As can be seen in Table 7, the situation at the comfort level for overhanging floors with a slenderness L_c/6 and an adjacent span of L_e=4L_c (slenderness L_e/24) is substantially better than that with an adjacent span of L_e=0.75 m. For an adjacent span of L_e=4L_c a comfort level II was obtained in all cases, both for multi-storey buildings for residential use and for offices, with total loads of up to 9.0 kN/m^2. This comfort level II corresponds to quality choice performance, according to Table 5. This means that the range of slenderness considered leads, regarding to vibrations, to high levels of comfort in use.

4. Conclusions

The behavior of timber-concrete composite floors in an overhanging configuration consisting of a prefabricated T-shape piece formed by a GLT flange glued to a plywood rib and connected to an upper concrete slab poured in situ has been analysed.

Three-point bending tests were performed with a total of 8 specimens obtained using the undamaged extreme quarters of the beams tested in previous four-point bending tests. All specimens were tested with a length-to-depth ratio equal to 6 (3 specimens of 1.50 m span and 25 cm height, 3 of 1.80 m and 30 cm and 2 of 2.10 m and 35 cm).

The results obtained indicate that possible hidden damages not detected would not be meaningful enough to significantly affect the results obtained and, in any case, would still make the results obtained more favourable.

The ultimate load values obtained for L_c=1.50 m were 9.90 and 7.18 times the design load considered for residential buildings (Q_{total}=5.0 kN/m^2) and for public use (Q_{total}=9.0 kN/m^2), respectively. In the case of L_c=1.80 m, these coefficients become 8.21 and 5.80. Finally, for L_c=2.10 m, values of 8.03 and 5.55 are obtained. All this demonstrates the high bearing capacity of the solution.

Two types of failure have been observed after a marked cracking process in the concrete when approaching the ultimate load value. Tensile failure affecting the plywood rib, produced in three of the eight specimens, and shear failure at the glulam interface flange-plywood rib joint in the remaining pieces. The load values that led to both types of failure were very similar, which indicates a fairly tight dimensioning of the elements that make up the section, as there was not a single resistant mechanism that precipitated the failure.

The most unfavorable deflection values obtained for the design load considered for residential buildings (Q_{total}=5.0 kN/m^2) and for public use (Q_{total}=9.0 kN/m^2) have been L_c/ 358 and L_c/266 for specimens 250 mm thick and with a span of 1.50 m; L_c/424 and L_c/309 for specimens of 300 mm and L_c=1.80 m; L_c/406 and L_c/289 for specimens of 350 mm

and L_c=2.10 m. These results amply satisfy both requirements usually associated with the assessment of integrity of the construction elements and that of user comfort.

The numerical models for vibrations made with a slenderness L_c/6 and an adjacent span *of L_e=4L_c* with total loads of up to 9.0 kN/m^2, both in multi-storey buildings for residential and public use, presented level II comfort corresponding to quality choice performance.

Although the number of full-scale prototypes tested is not high enough to have adequate statistical reliability and it should prevent from drawing definitive conclusions, the ultimate load reached in all the tests, and the uniformity of results in terms of stiffness that amply satisfy rules requirements, support the feasibility and interest of using the system developed in the field of negative bending moments behaviour.

5. Author statement

All the authors have actively participated in the different phases of development, both in the experimental phase described and in the preparation of the materials included in the article.

Declaration of Competing Interest

The authors declare that they have no known competing financial interests or personal relationships that could have appeared to influence the work reported in this paper.

Data availability

Data will be made available on request.

Acknowledgments

References

[1] United Nations Environment Programme. Global status report for buildings and construction. Towards a zero-emissions, efficient and resilient buildings and construction sector. Nairobi (2021). http://globalabc.org/resources/publications.

[2] International Energy Agency. Energy Efficiency 2021, OECD Publishing, Paris (2021). https://doi.org/10.1787/cfb80e1e-en.

[3] Stocchero A, Seadon JK, Falshaw R, Edwards M. Urban equilibrium for sustainable cities and the contribution of timber buildings to balance urban carbon emissions: A New Zealand case study. J Clean Prod 2017;143:1001–10. https://doi.org/10.1016/j.jclepro.2016.12.020.

[4] Andersen JH, Rasmussen NL, Ryberg MW. Comparative life cycle assessment of cross laminated timber building and concrete building with special focus on biogenic carbon. Energy Build 2022;254:111604.

[5] Li J, Rismanchi B, Ngo T. Feasibility study to estimate the environmental benefits of utilising timber to construct high-rise buildings in Australia. Build Environ January 2019;147:108–20. https://doi.org/10.1016/j.buildenv.2018.09.052.

[6] Hassan OAB, Öberg F, Gezelius E. Cross-laminated timber flooring and concrete slab flooring: A comparative study of structural design, economic and environmental consequences. J Build Eng 2019;26:100881.

[7] Organisation for Economic Cooperation and Development. Global Material Resources Outlook to 2060: Economic Drivers and Environmental Consequences. OECD Publishing, Paris (2019). https://doi.org/10.1787/9789264307452-en.

[8] Ahmad A, Liu Q, Nizami SM, Mannan A, Saeed S. Carbon emission from deforestation, forest degradation and wood harvest in the temperate region of Hindukush Himalaya, Pakistan between 1994 and 2016. Land Use Policy 2018;78: 781–90. https://doi.org/10.1016/j.landusepol.2018.07.009.

[9] Knauf M. Market potentials for timber-concrete composites in Germany's building construction sector. Eur J Wood Wood Prod 2017;75:639–49. https://doi.org/10.1007/s00107-016-1136-9.

[10] Dias A, Skinner J, Crews K, Tannert T. Timber-concrete-composites increasing the use of timber in construction. Eur J Wood Wood Prod 2016;74:443–51. https://doi.org/10.1007/s00107-015-0975-0.

[11] Yeoh D, Fragiacomo M, De Franceschi M, Heng Boon K. State of the Art on Timber-Concrete Composite Structures: Literature Review. J Struct Eng 2011;137(10): 1085–95. https://doi.org/10.1061/(ASCE)ST.1943-541X.0000353.

[12] Estévez-Cimadevila J, Martín-Gutiérrez E, Suárez-Riestra F, Otero-Chans D, Vázquez-Rodríguez JA. Timber-concrete composite structural flooring system. J Build Eng 2022;49:104078. https://doi.org/10.1016/j.jobe.2022.104078.

[13] Otero-Chans D, Estévez-Cimadevila J, Suárez-Riestra F, Martín-Gutiérrez E. Perforated board shear connector for timber-concrete composites. Wood Mater Sci Eng 2023;18(3). https://doi.org/10.1080/17480272.2022.2089594.

[14] Martín-Gutiérrez E, Estévez-Cimadevila J, Suárez-Riestra F, Otero-Chans D. Flexural behavior of a new timber-concrete compostie structural flooring system. Full scale testing. Journal of Building. Engineering 2023;64:105606. https://doi.org/10.1016/j.jobe.2022.105606.

[15] Kuhlmann U, Schänzlin J. A Timber–Concrete Composite Slab System for Use in Tall Buildings. Struct Eng Int 2008;18(2):174–8. https://doi.org/10.2749/101686608784218707.

[16] Sebastian W, Lawrence A, Smith A. Commentary: The potential for multi-span continuous timber–concrete composite floors. Proc Inst Civil Eng - Struct Build 2018;171(9):661–2. https://doi.org/10.1680/jstbu.171.9.661.

[17] EN 14080:2013. Timber structures. Glued laminated timber and glued solid timber. Requirements. European Comittee for Standardization. Brussels.

[18] UNE 36068:2011. Ribbed bars of weldable steel for the reinforcement of concrete. Aenor. Madrid.

[19] EN 197-1:2011. Cement - Part 1: Composition, specifications and conformity criteria for common cements. European Committee for Standardization. Brussels.

[20] EN 14889-2:2008. Fibres for concrete. Part 2: polymer fibres. Definitions, specifications and conformity. European Committee for Standardization. Brussels.

[21] UNE-EN 12350-2:2020 Testing fresh concrete - Part 2: Slump test. European Committee for Standardization. Brussels.

[22] EN 12390-3:2019. Testing hardened concrete. Part 3: compressive strength of test specimens. European Committee for Standardization. Brussels.

[23] EN 1995-1-1:2016. Eurocode 5. Design of timber structures. European Committee for Standardization. Brussels.

[24] Dias A, Schänzlin J, Dietsch P (eds.). Design of timber-concrete composite structures: A state-of-the-art report by COST Action FP1402 / WG 4, Shaker Verlag Aachen, 2018.

[25] Khorsandnia N, Valipour HR, Crews K. Structural response of timber-concrete composite beams predicted by finite element models and manual calculations. 2013 World Congress on Advances in Structural Engineering and Mechanics (ASEM13). Korea; 2013.

[26] EN 1991-1-1. Eurocode 1: Actions on structures. European Committee for Standardization. Brussels, 2002.

[27] UNE-EN 1992-1-1 Eurocode 2: Design of concrete structures. Part 1-1: General rules and rules for buildings. European Committee for Standardization. Brussels. 2021.

[28] EN 1990:2002/A1: 2005. Eurocode. Basis of structural design. European Committee for Standardization. Brussels, 2005.

[29] ISO 10137:2007. Bases for design of structures - Serviceability of buildings and walkways against vibrations.

[30] ISO 2631-1:2008. Mechanical vibration and shock. Evaluation of human exposure to whole-body vibration. Part 1: General requirements.

[31] EN 1995-1-1. Project team SC5.T3. Sub-task 7. Vibrations. Milestone 2. European Committee for Standardization. Brussels, 2019.

[32] Feldmann M, et al., EUR 28084 EN. Design of floor structures for human induced vibrations. Background document in support to the implementation, harmonization and further development of the Eurocodes. Joint Research Centre, Institute for the Protection and Security of the Citizen. Publications Office of the European Union, 2011. https://doi.org/10.2788/4640.